RESEARCH ARTICLE

L-Norvaline, a new therapeutic agent against Alzheimer's disease

Baruh Polis[1, 2, *], **Kolluru D. Srikanth**[2], **Vyacheslav Gurevich**[3], **Hava Gil-Henn**[2], **Abraham O. Samson**[1]
1 Drug Discovery Laboratory, The Azrieli Faculty of Medicine, Bar-Ilan University, Safed, Israel
2 Laboratory of Cell Migration and Invasion, The Azrieli Faculty of Medicine, Bar-Ilan University, Safed, Israel
3 Laboratory of Cancer Personalized Medicine and Diagnostic Genomics, The Azrieli Faculty of Medicine, Bar-Ilan University, Safed, Israel

Funding: *This research was supported by Marie Curie CIG Grant 322113, Leir Foundation Grant, Ginzburg Family Foundation Grant, and Katz Foundation Grant (all to AOS).*

Abstract

Growing evidence highlights the role of arginase activity in the manifestation of Alzheimer's disease (AD). Up-regulation of arginase was shown to contribute to neurodegeneration. Regulation of arginase activity appears to be a promising approach for interfering with the pathogenesis of AD. Therefore, the enzyme represents a novel therapeutic target. In this study, we administered an arginase inhibitor, L-norvaline (250 mg/L), for 2.5 months to a triple-transgenic model (3×Tg-AD) harboring PS1M146V, APPSwe, and tauP301L transgenes. Then, the neuroprotective effects of L-norvaline were evaluated using immunohistochemistry, proteomics, and quantitative polymerase chain reaction assays. Finally, we identified the biological pathways activated by the treatment. Remarkably, L-norvaline treatment reverses the cognitive decline in AD mice. The treatment is neuroprotective as indicated by reduced beta-amyloidosis, alleviated microgliosis, and reduced tumor necrosis factor transcription levels. Moreover, elevated levels of neuroplasticity related postsynaptic density protein 95 were detected in the hippocampi of mice treated with L-norvaline. Furthermore, we disclosed several biological pathways, which were involved in cell survival and neuroplasticity and were activated by the treatment. Through these modes of action, L-norvaline has the potential to improve the symptoms of AD and even interferes with its pathogenesis. As such, L-norvaline is a promising neuroprotective molecule that might be tailored for the treatment of a range of neurodegenerative disorders. The study was approved by the Bar-Ilan University Animal Care and Use Committee (approval No. 82-10-2017) on October 1, 2017.

Correspondence to:
Baruh Polis, MD,
baruhpolis@gmail.com.

orcid:
0000-0002-3496-8250
(Baruh Polis)

doi: *10.4103/1673-5374.255980*

Received: *December 4, 2018*
Accepted: *March 1, 2019*

Key Words: *dementia; arginase inhibition; arginine; urea cycle; microgliosis; neuroinflammation; cytokines; tumor necrosis factor; mTOR; neurodegeneration*

Chinese Library Classification No. *453; R364*

Introduction

Alzheimer's disease (AD) is the primary cause of dementia presenting a severe health problem for the elderly and a growing economic burden for society. AD-associated dementia is characterized morphologically by neuritic plaques containing amyloid-beta (Aβ) peptide and neurofibrillary tangles that are aggregates of hyperphosphorylated tau protein (Schaeffer et al., 2011). The currently dominant amyloid hypothesis of AD pathogenesis postulates that accumulation of Aβ in the brain is the principal cause of AD development (Selkoe and Hardy, 2002). Several therapeutic protocols, predicated upon the hypothesis, have been trialed in AD patients. Unfortunately, all finalized experiments have failed to improve the cognitive functions of AD patients. Moreover, some trials were terminated due to adverse effects (Doody et al., 2013; Lahiri et al., 2014).

Failure to meet the clinical endpoints with the traditional anti-amyloid approaches led to rigorous investigations of other AD-related histopathologies, including microgliosis and astrogliosis. These features characterize AD in a region- and time-dependent manner (Osborn et al., 2016). Moreover, activated microglia produce pro-inflammatory mediators in response to Aβ, which in turn activate astrocytes and eventually lead to neuropathology (Heneka et al., 2015). Therefore, dysregulation of cytokine signaling contributes to AD-associated learning and memory deficiency and synaptic dysfunction (Morris et al., 2013). Consequently, results showing improvement of the memory deficiency in rodents with manipulated microglial proliferation have been published recently (Spangenberg et al., 2016).

Contemporary studies indicate that urea cycle disordering plays a role in the pathogenesis of AD (Kan et al., 2015). Specifically, the brains of AD patients show significantly upregulated arginase activity, and reduced nitric oxide synthase activity (Liu et al., 2014), which is followed by a decrease in the levels of their mutual substrate - L-arginine (Gueli and Taibi, 2013). Moreover, the brains of AD patients, in comparison to healthy brains, contain significantly higher concentrations of urea, which is a waste product of the reaction catalyzed by arginase (Xu et al., 2016a).

Our previous report associated local amyloid-beta-driven immune-mediated response with altered L-arginine metabolism, and suggested that arginase inhibition by L-norvaline interrupts the progression of AD (Polis et al., 2018). Accordingly, we hypothesized that dysregulation of the urea cycle in the brain, with upregulation of arginase and consequent nitric oxide and L-arginine deficiency, leads to the clinical manifestation of AD pathology. Additionally, we suggest that brain accumulation of molecular waste products (*i.e.*, urea) is a central pathological process, which leads to neuroinflammation and disrupts efficient communication between neurons. Therefore, arginase is a potential target for treating AD.

To verify our hypothesis, we used an arginase inhibitor, L-norvaline, in a murine model of AD and applied a set of immunohistochemistry, proteomics, and quantitative polymerase chain reaction assays. Bioinformatics analysis was utilized to identify the involved biological pathways.

Materials and Methods

Strains of mice and treatment

Homozygous triple-transgenic mice (3×Tg-AD) harboring PS1(M146V), APP(Swe), and tau(P301L) transgenes were purchased from Jackson Laboratory (Bar Harbor, ME, USA) and bred in our animal facility. These animals exhibit a synaptic deficiency, plaque, and tangle pathology (Oddo et al., 2003).

Male 4-month-old homozygous 3×Tg-AD mice weighing about 30 g were randomly divided into two groups (13 mice in each group). The animals were housed in cages (5 mice per cage) and provided with water and food *ad libitum*. The control animals received regular water. The experimental mice received water with dissolved L-norvaline (Sigma, St. Louis, MO, USA) (250 mg/L). The experiment lasted 2.5 months. The Bar-Ilan University Animal Care and Use Committee approved the experimental protocol (approval No. 82-10-2017) on October 1, 2017. The research was done in accordance with the "Guide for the Care and Use of Laboratory Animals" developed by National Research Council (US) Committee for the Update of the Guide for the Care and Use of Laboratory Animals and "The Guidelines for the Care and Use of Mammals in Neuroscience and Behavioral Research" developed by National Research Council (US) Committee on Guidelines for the Use of Animals in Neuroscience and Behavioral Research.

Fear conditioning test

Contextual fear conditioning is a form of associative learning, in which an animal learns to associate the neutral conditioned stimulus, with the presence of a motivationally significant unconditioned stimulus, such as an electric shock (Wehner and Radcliffe, 2004). In this paradigm, the freezing behavior represents a typical natural response in rodents. The easily assessable lack of movement provides a readout of the memory acquisition and reflects the integrity of the hippocampus (Anagnostaras et al., 2001).

The experiments were performed using two standard chambers with shock floors purchased from Noldus® (Wageningen, The Netherlands). Each chamber had a 17 cm × 17 cm floor and is 30 cm in height and was equipped with a top unit including a matrix of infrared lights and an infrared camera, with a high-pass filter blocking visible light. The floor of the chambers included a stainless steel grid (inter-bar separation 0.9 cm) connected to an electric shock generator(Ugo Basile SRL, Gemonio VA, Italy). Automated tracking was done with EthoVision XT 10 software also provided by Noldus® (Wageningen, The Netherlands). Mice were handled for 3 successive days for 5 minutes a day. During day one, an animal was placed in a chamber for 5 minutes and exposed to white background noise. Initial habituation period (**Figure 1A**) on the first day allowed acclimation to the experimental environment and reduction of orienting responses. Freezing behavior of the mice was tested 24 hours after training.

On the second day of a conditioning session, mice received two 2-second long 0.75 mA foot shocks, at 3.0 and 4.5 minutes after placement into the chamber. On the third day of the testing session, mice were exposed for 5 minutes to the same conditioning context without a shock.

Tissue sampling

After behavioral experiments, the animals were decapitated with scissors. Fresh brain sections (0.5 mm thick) between 1.7 mm and 2.2 mm posterior to bregma (by the atlas of Franklin and Paxinos) were collected for sampling (Franklin and Paxinos, 2007). The hippocampi were perforated at the dentate gyrus with a 13-gauge dissection needle (Fisher Scientific, Hampton, New Hampshire, USA). The brain punched tissues were frozen and stored at –80°C.

Pathway enrichment analysis

To identify specific biomarkers and signatures of phenotypic state caused by L-norvaline treatments in 3×Tg-AD mice, we accomplished a functional interpretation of the genes derived from the antibody microarray assay done in the previous study (Polis et al., 2018). The array includes 1448 targets. There are 84 significantly up and down-regulated proteins with significant (P-value < 0.05) change of expression in the rate more than 25% (**Additional Table 1**). The pathway enrichment analysis was performed using Ingenuity® Pathway Analysis software (IPA®) (QIAGEN, Germantown, MD, USA). The IPA® tool was applied to uncover the significance of proteomics data and identify candidate biomarkers within the context of 3×Tg-AD mice as a biological system.

Immunostaining

Four animals from each group were deeply anesthetized with intraperitoneal injection of Pental (0.2 mL; CTS Chemical Industries Ltd., Kiryat Malachi, Israel) and transcardially perfused with 30 mL of phosphate buffered saline (PBS), followed by 50 mL of chilled 4% paraformaldehyde in PBS. The brains, liver, and kidney were carefully removed and fixed in 4% paraformaldehyde for 24 hours. The organs were transferred to 70% ethanol at 4°C for 48 hours, dehydrated, and paraffin embedded. The paraffin-embedded blocks were ice-cooled and sliced at a thickness of 4 μm. The sections were mounted, dried overnight at room temperature, and stored at 4°C.

For the quantitative histochemical analysis of beta-amyloid, three coronal brain sections cut at 25 μm intervals throughout the brain per mouse (1.8–2.0 mm posterior to bregma) were used. Immunohistochemistry was performed on the plane-matched coronal sections.

The kidneys were sliced in half longitudinally, and the liver was cut in transverse sections. For the analysis of arginase 1 (ARG1) immunoreactivity in the liver and arginase 2 (ARG2) in the kidney, two 4 μm-thick sections were cut per organ at 100 μm intervals.

Staining was accomplished on a Leica Bond III system (Leica Biosystems Newcastle Ltd., Newcastle upon Tyne, UK). The

tissues pretreated with an epitope-retrieval solution (Leica Biosystems Newcastle Ltd.) were incubated with primary antibodies for 30 minutes. For the 6E10 (Abcam, #ab2539), ARG1 (GeneTex, #GTX113131), and ARG2 (GeneTex, #GTX104036) antibodies dilutions were 1:200, 1:500, 1:600 respectively. A Leica Refine-HRP kit (Leica Biosystems Newcastle Ltd.) served for hematoxylin counterstaining. The omission of the primary antibodies served as a negative control.

Imaging and quantification analysis

The sections were viewed under a slide scanner Axio Scan.Z1 (Zeiss, Oberkochen, Germany) with a 40×/0.95 objective. The images were captured at various focal distances (Z-planes) to provide a composite image with a greater depth of field (mostly at 0.5 μm). The image analysis was carried out using ZEN Blue 2.5 (Zeiss). A fixed background intensity threshold was set for all sections representing a single type of staining. For 6E10 staining, the analysis of immunoreaction was performed in the CA1, CA3, CA4 areas of the hippocampus. The surface of the immunoreactive area (above the threshold) has been subjected to the statistical analysis.

Additionally, the image densitometry method was applied to quantify the amount of staining in the specimens. Integrated optical density, which is the optical density of individual pixels in the image reflecting the expression levels of the proteins, was measured *via* digital image analysis software (Image-Pro® 10.0.1; Media Cybernetics, Inc., Rockville, MD, USA), and presented as the average value for each treatment group.

The glomerular area was quantified using ZEN Blue 2.5. Twenty-four cortical glomeruli were measured in each group. In order to ensure that chosen glomeruli were sectioned in the same plane, only those containing evident efferent and afferent arteriolar stalks have been analyzed. Bowman's capsule diameters were statistically compared.

RNA extraction, reverse transcription, and real-time polymerase chain reaction

Hippocampal tissues were sampled from five animals (each group). Total RNA was isolated using the RNeasy Mini Kit (Cat# 74104, QIAGEN) following the manufacturer's instructions including DNase treatment. RNA quantification was performed using Qubit™ RNA HS Assay Kit (Cat# Q32852, Invitrogen, Carlsbad, CA, USA). RNA integrity (RIN) was measured using Agilent 2100 Bioanalyzer System and Agilent RNA 6000 Pico Kit (Cat# 5067-1513, Agilent Technologies, Santa Clara, CA, USA). cDNA was prepared from 200 ng of total RNA using SuperScript® III First-Strand Synthesis System for real-time polymerase chain reaction (RT-PCR) (Cat# 18080-051, Invitrogen) following the manufacturer's instructions. Real-time PCR was performed using TaqMan Tnf: Mm00443258_m1 (Applied Biosystems, Foster City, California, USA) probe. For the normalization of tumor necrosis factor (TNF)-α RNA levels, ACTB and GAPDH endogenous housekeeping genes controls were analyzed using ActB: Mm00607939_s1 and Gapdh: Mm99999915_g1 probes respectively. PCR was set in triplicates following the manufacturer's instructions (Applied Biosystems, Insert PN 4444602 Rev. C) in a 10 μL volume using 5 ng cDNA template. PCR was run, and the data was analyzed in the StepOnePlus system installed with StepOne Software v2.3 (Applied Biosystems). The quantification was performed using the comparative Ct (ΔΔCt) method (Livak and Schmittgen, 2001).

Western bolt assay

Hippocampal tissue was homogenized in an equal ratio of tissue homogenate buffer (50 mM Tris-HCl (pH 7.5), 150 mM KCl, 0.32 M sucrose, Protease inhibitor cocktail (Sigma)) and lysis buffer (1% Triton, 10% glycerol, 120 mM NaCl, 25 mM 4-(2-hydroxyethyl)-1-piperazineethanesulfonic acid, 1 mM ethylenediaminetetraacetic acid EDTA, 0.75 mM $MgCl_2$, 2 mM NaF, 1 mM sodium vanadate & protease inhibitor). The samples were incubated on ice for 10 minutes and centrifuged at 11,000 × *g* for 10 minutes at 4°C. The supernatant was aliquoted, and protein concentration was determined using a protein assay kit (Bio-Rad, Hercules, CA, USA). Forty μg samples were subjected to sodium dodecyl sulfate polyacrylamide gel electrophoresis and transferred onto nitrocellulose membranes. The membranes were blocked for 1 hour at room temperature in Tris-buffered saline containing 0.1% casein. The membranes were incubated overnight at 4°C with primary antibody 1:500 dilution of postsynaptic density protein 95 (PSD-95) (Abcam, ab18258), beta-secretase 1 (BACE-1) (Abcam, ab2077), amyloid precursor protein (APP) (Abcam, ab2072). Following washing with Tris buffered saline with Tween, the membranes were incubated with LI-COR dye-conjugated secondary antibody (IRDye® 680RD; LI-COR Biosciences, Lincoln, NE, USA) for 1 hour at 22°C. The beta-actin antibody was used as a reference under the same conditions (Abcam, ab8227) at 1:5000 dilution. Membranes were scanned on the Odyssey® CLx Imager (LI-COR Biosciences).

Statistical analysis

Statistical analyses were conducted with GraphPad Prism 7.0 for Windows (GraphPad Software, San Diego, CA, USA). The significance was set at 95% of confidence. The two-tailed Student's *t*-test was performed to compare the means. All data are presented as mean values. Throughout the text and in plots, the variability is indicated by the standard error of the mean (SEM).

Results

L-Norvaline improves memory acquisition in the 3×Tg-AD mice

The animals treated with L-norvaline exhibited significantly increased freezing time during the fourth ($P = 0.033$) and fifth ($P = 0.018$) minutes of the test compared to the control group (**Figure 1C**). Taking into account that the experimental animals were exposed to the shocks only during the second part of the procedure (**Figure 1B**), we concluded that their contextual memory acquisition, which is associated with the conditioned stimulus, improved significantly following the treatment with L-norvaline.

L-Norvaline reduces β-amyloidosis in the hippocampi of 3×Tg-AD mice

Coronal brain sections of the 3×Tg-AD mice were stained with anti-β-amyloid antibody (6E10) to study the impact of the L-norvaline treatment on the amyloid burden. Six- to seven-month-old 3×Tg-AD mice exhibited enhanced intracellular and extracellular deposition of Aβ in their hippocampi (**Figure 2A** and **B**). Intracellular deposits were most prominent in the CA1 area (**Figure 2C**), with a substantial reduction in the L-norvaline treated group (**Figure 2D**). Only a few plaques were detected within the hippocampi. The analysis of immunoreactive surface area was performed in the CA1 (**Figure 2C** and **D**), CA3 (**Figure 2E** and **F**), and CA4 regions of the hippocampi. We detected significant differences in the levels of immunoreactivity between the two experimental groups. There was a significant reduction in the 6E10 immunoreactivity in the CA1 ($P = 0.0095$), CA3 ($P = 0.016$), CA4 ($P = 0.016$) areas. These data point to an effect of L-norvaline on the level of β-amyloidosis in the 3×Tg-AD mice and support our previously reported findings (Polis et al., 2018).

L-Norvaline reduces the transcription levels of TNFα gene

Tumor necrosis factor signaling is required for Aβ-induced neuronal death (Chang, et al. 2017). The critical role of TNFα in AD pathogenesis is supported by observations made in the mouse models of AD (Sly et al., 2001). Elevated TNFα levels were observed in the brain tissues of AD transgenic mice. To investigate the impact of L-norvaline treatment on TNFα gene expression levels, mRNA was isolated from the hippocampi of control and treated mice, and analyzed by quantitative RT-PCR. cDNA levels were normalized to the reference genes GAPDH and ACTB and presented relative to gene expression in vehicle controls. The two-tailed Student's *t*-test ($t = 2.66$, $df = 8$) revealed a significant ($P = 0.029$) reduction (by 35.5%) of TNFα gene expression levels in the L-norvaline treated group (**Figure 3**).

L-Norvaline amplifies the expression levels of postsynaptic density-95 protein in the 3×Tg-AD mice

The impact of the L-norvaline treatment upon the hippocampal levels of neuroplasticity-associated protein PSD-95 in the 3×Tg-AD mice was investigated using western blotting. Decreased levels of PSD-95 in the cerebral cortex and hippocampus of 3×Tg-AD mice compared to the WT mice were previously reported (Revilla et al., 2014a), suggesting synaptic integrity loss in this model. We previously analyzed the effect of L-norvaline upon the spine density and the expression levels a list of neuroplasticity related proteins. We disclosed a relative spine deficiency in the 3×Tg-AD mice compared to WT and evidenced an increase in spine density (by ~20%) following the treatment (Polis et al., 2018).

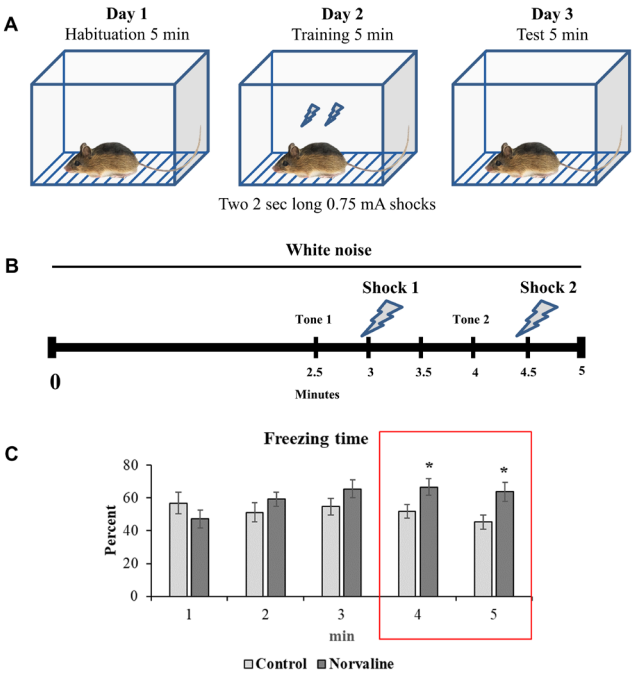

Figure 1 Contextual fear conditioning.

(A) Experimental design. (B) Fear training scheme. (C) Effect of L-norvaline treatment on freezing time during the 5-minute test. Mean freezing levels (± SEM) of controls ($n = 13$) and L-norvaline treated mice ($n = 13$) are recorded. The two-tailed Student's *t*-test revealed a significant effect of the treatment on freezing time, $*P < 0.05$. Red box indicates the periods of time with significant differences in freezing behavior between the groups).

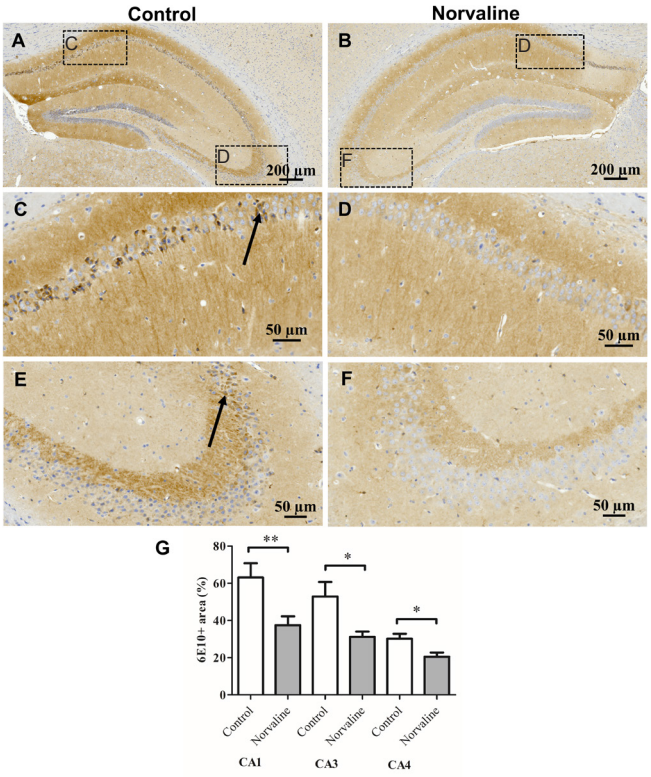

Figure 2 The effect of L-norvaline on the hippocampal Aβ burden in the 3×Tg-AD mice.

Representative 40× photomicrographs of the entire hippocampi stained with anti-Aβ 6E10 antibody from the control (A) and L-norvaline treated (B) mice. Insets C and D represent the CA1 region, E and F represent CA3 region. Arrows indicate the cells with dense amyloid deposition. Quantification of the Aβ-immunoreactive area in different brain regions of the 3×Tg-AD mice treated with vehicle (control) or L-norvaline (G). Data are presented as the mean ± SEM (two-tailed Student's *t*-test). $*P < 0.05$, $**P < 0.01$ ($n = 12$ brain sections, three mice per group). Aβ: Amyloid-beta.

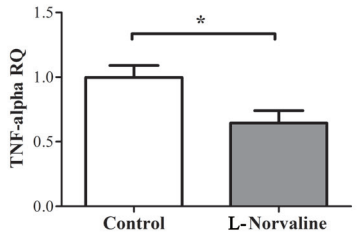

Figure 3 Hippocampal TNFα mRNA expression levels.
Real-time polymerase chain reaction analysis of mRNA levels of TNFα gene. All data are presented as the mean ± SEM ($n = 5$ brain sections per group). $*P < 0.05$ (two-tailed Student's t-test). TNF: Tumor necrosis factor.

To evaluate further the effect of the treatment on synaptic integrity, we measured the levels of the post-synaptic protein PSD-95. We observed a significant ($P = 0.015$) increase (by 17.2%) in PSD-95 levels in the hippocampi of 3×Tg-AD mice treated with L-norvaline compared to the control animals (**Figure 4A**), which accords with the data acquired by Golgi staining analysis and reported previously (Polis et al., 2018).

L-Norvaline reduces the expression levels of APP but not BACE-1 in the 3×Tg-AD mice

The brains of 3×Tg-AD mice contain growing with age APP levels, which are higher than in WT animals (Croft et al., 2017). Immunohistochemistry with 6E10 antibody revealed a significant reduction of the total amyloid burden in the cortices and hippocampi of mice treated with L-norvaline. To comprehend the phenomenon and address it to the moderated transcription of APP or altered processing by BACE-1, we performed western blot analysis of the extracted proteins. Quantitative analysis of the blots demonstrated that L-norvaline significantly ($P = 0.029$) reduced (by 43%) the levels of APP expression (**Figure 4B**), however, it had little or no effect ($P = 0.59$) on the levels of BACE-1 protein (**Figure 4C**).

L-Norvaline induces cellular pathways involved in neuroplasticity and oxidative stress protection

The pathway enrichment analysis with a preset threshold of 25% change from control and the significance set at 95% of confidence revealed that treatment of 3×Tg-AD mice with L-norvaline led to activation of 41 critical biological processes (**Figure 5**). Among the most significant pathways (with $P < 0.0025$ and overlap > 30%) detected by IPA® were neuregulin pathway, synaptic long-term depression, ERK/MAPK pathway, and oncostatin M pathway. Moreover, IPA® points out several signaling pathways with significant effect, which are involved in cell survival and immune response. Among them are PI3K/AKT signaling, TREM1 signaling, CDK5 signaling, IL-2, IL-3, IL-15 signaling.

Neuregulins comprise a cluster of epidermal growth factor-like proteins that act on the epidermal growth factor receptor family of receptors and are highly implicated in neural development and brain homeostasis (Mei and Nave, 2014). Accumulating evidence suggests that neuregulin-1 signaling has an impact on cognitive function and neuropathology in AD. Overexpression of neuregulin-1 in the

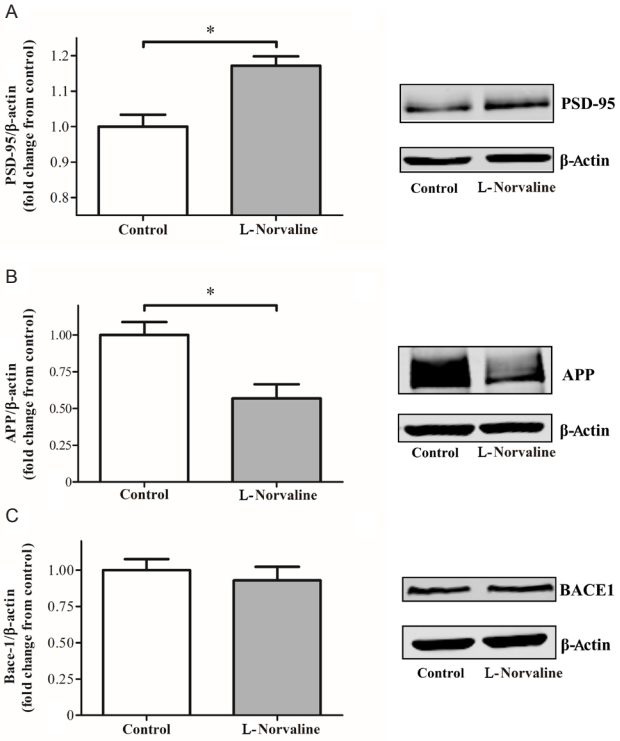

Figure 4 Hippocampal protein expression of PSD-95 (A), APP (B), and BACE-1 (C: western blot assay).
Western blot band intensities normalized with their respective β-actin bands were compared and presented by bar charts as fold change from vehicle-treated controls. PSD-95 expression levels are significantly higher and APP lower in the brains of L-norvaline mice. There is no significant effect of the treatment upon the levels of BACE-1 protein (data are mean ± SEM, $*P < 0.05$, two-tailed Student's t-test, $n = 3$ brain sections per group). PSD-95: Postsynaptic density protein 95; APP: Amyloid precursor protein; BACE-1: beta-secretase 1.

hippocampus of AD mice improves memory deficits and ameliorates disease-associated neuropathology (Xu et al., 2016b). Our results reveal upregulation of several important downstream to neuregulin proteins. We demonstrate that the levels of Src proto-oncogene-encoded protein-tyrosine kinase increase significantly ($P = 0.003$) by 94% in the brains of the treated group. Src activity was shown to be required for avoidance memory formation and recall (Bevilaqua et al., 2003). Moreover, the levels of signal transducer and activator of transcription 5A (STAT5) escalated significantly ($P = 0.006$) by 45%. STAT5 is an essential cellular mechanism regulating cognitive functions. Brain-specific STAT5 ablation was shown recently to impair learning and memory formation in mice (Furigo et al., 2018). Another study suggests a contribution of STAT5 in neuroprotection (Zhang et al., 2007). The authors demonstrate a strong association between STAT5 activation and neuronal survival in the rat hippocampus after cerebral ischemia.

The platelet-derived growth factor (PDGF) ligands and receptors are expressed during embryonic development and in the mature nervous system. In pathologic conditions, PDGF modulates neuronal excitability and stimulates survival signals, *via* the PI3-K/Akt pathway and other ways, rescuing cells from apoptosis (Funa and Sasahara, 2014). PDGF

signaling defects have been shown to underlie the clinical progression of neurodegeneration in multiple sclerosis (Mori et al., 2013). Our assay confirms that PDGF signaling is highly involved and activated by L-norvaline treatment (P = 0.00025). The levels of one of the central enzymes of the pathway, sphingosine kinase 2, increased significantly (P = 0.036) by 56% following the treatment. Sphingosine kinase 2 is highly implicated in AD pathogenesis as indicated by dysregulation of the sphingolipid metabolism (*i.e.*, reduced levels of sphingosine 1-phosphate, a product of the reaction) in AD brains (Dominguez et al., 2018). Sphingosine 1-phosphate is a potent neuroprotective signaling lipid (Couttas et al., 2014), which acts *via* specific G protein-coupled receptors (S1PRs) and regulates microglial number and activity in the brain (Hla and Brinkmann, 2011).

Vascular endothelial growth factor is essential for neuroprotection (Rosenstein et al., 2010). Vascular endothelial growth factor signaling activation is particularly beneficial in individuals showing early hallmarks of AD (Hohman et al., 2015). We demonstrate that L-norvaline significantly (P = 0.004) up-regulates vascular endothelial growth factor signaling pathway in the 3×Tg-AD mice. L-Norvaline treatment additionally leads to up-regulation of the ERK/MAPK signaling pathway, which is essential for endogenous neuroprotection (Karmarkar et al., 2011). Moreover, IPA® points out other pathways with significant effect, which are involved in cell survival and immune response.

Noteworthy, L-norvaline treatment led to a significant (P = 0.04) increase (by 53%) in the levels of glial cell-derived neurotrophic factor (GDNF) receptor Ret, as detected by the antibody array. Ret is a tyrosine kinase and common signaling receptor for GDNF-family ligands (Airaksinen and Saarma, 2002). Generally, GDNF is an effective supporter of neuronal survival (Allen et al., 2013), and Ret is essential for mediating GDNF neuroprotective and neuroregenerative effects (Drinkut et al., 2016). Moreover, neural cell adhesion molecule, which has been identified as a second signaling receptor for GDNF (Paratcha et al., 2003), demonstrated a significantly (P = 0.003) elevated (by 43%) levels following the treatment. Neural cell adhesion molecule regulates synaptic plasticity (Lüthi et al., 1994), and mediates the axonal growth in the hippocampal and cortical neurons (Paratcha et al., 2003). Of note, GDNF is down-regulated in 7-month-old 3×Tg-AD mice (Revilla et al., 2014a) and GDNF overexpression improves learning and memory in this model of AD (Revilla et al., 2014b).

Additionally, L-norvaline treatment led to a substantial increase (by 59%) in the levels of protein-serine kinase suppressor of Ras 1 (Ksr1), which is critical for neuroprotection. Ksr1 mediates the anti-apoptotic effects of brain-derived neurotrophic factor (Szatmari et al., 2007), which is highly implicated in AD (Peng et al., 2005).

Contemporary data demonstrate that another essential neuroprotective factor, nerve growth factor, plays a crucial role in normal aging (Parikh et al., 2013) and AD pathogenesis (Iulita and Cuello, 2014). Consequently, nerve growth factor application has emerged as a novel approach for AD therapy (Eyjolfsdottir et al., 2016). Of note, the neuroprotective effects of nerve growth factor are mediated *via* tropomyosin receptor kinase A (Nguyen et al., 2010), which was significantly (P = 0.039) increased (by 56%) following the treatment.

Antibody microarray detected several other essential for cell survival proteins that demonstrated a significant but moderate (less than 25% cutoff for IPA®) escalation rate following the treatment. For example, superoxide dismutase [Cu-Zn] levels were elevated by 19% in the brains of the treated animals. This enzyme plays a critical role in cellular response to oxygen-containing compounds and has been shown to be neuroprotective in a rat model with N-methyl-D-aspartic acid-induced excitotoxic injury (Peluffo et al., 2006). Additionally, we observed a 24% increase in the levels of phosphatidylinositol 3-kinase regulatory subunit alpha, which protects against H_2O_2-induced neuron degeneration (Yu et al., 2004). Accordingly, we suggest that L-norvaline possesses several converging on neuroprotection modes of activity (**Figure 6**).

L-Norvaline effectively reduces the expression levels of ARG1 and ARG2 in the primary organs of their activity without inducing morphological aberrations

In order to evaluate the rate of ARG1 inhibition by L-norvaline in the hepatic tissue, we performed a histological analysis of the 3×Tg-AD mice liver. We did not detect structural changes of the classical hexagonal, divided into concentric parts, hepatic lobular structure following the treatment (**Figure 7A–D**). However, the levels of ARG1 immunoreactivity were significantly reduced in the L-norvaline treated group, which was reflected by a decrease in ARG1 immunoreactive surface area (P = 0.015) and integrated optical density (P = 0.04).

Additionally, we performed renal tissue staining with ARG2 antibody and hematoxylin to assess the kidney structural integrity and the levels of ARG2 expression following the L-norvaline treatment. It was shown previously in the rat, that ARG2 is intensely expressed in the proximal straight tubules of outer medulla, and a subpopulation of the proximal tubules of the renal cortex (Miyanaka et al., 1998). Our data accord with these findings (**Figure 8**).

In previous studies, the Bowman's capsule space expansion was marked as a central histological kidney's dysfunction characteristic (Thakur et al., 2006; Tobar et al., 2013).

We subjected the cortical glomerular capsule diameter to the statistical analysis to detect deviations in glomerular space. We did not observe any significant variability (P = 0.081) in the Bowman's capsule diameters between experimental groups (**Figure 8F**). The mean diameters were 95.15 ± 1.88 μm in the control group and 99.97 ± 1.93 μm in the treated group. Nevertheless, the ARG2 immunoreactivity was significantly (P < 0.001) reduced in the treated with L-norvaline mice (**Figure 8E**).

Discussion

In this study, we continued the investigation of neuroprotective properties of a non-proteinogenic amino acid

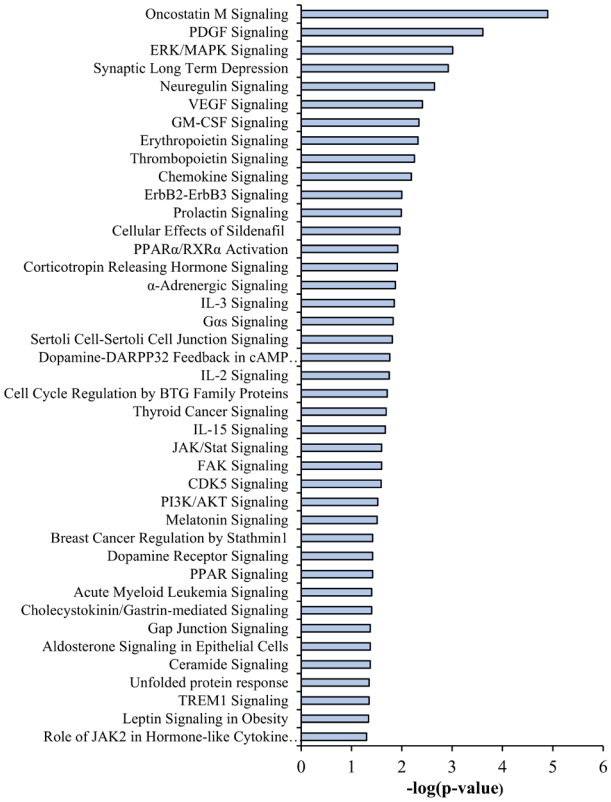

Figure 5 Ingenuity pathway analysis (IPA®) of differentially expressed genes.
The microarray data with expression levels of more than one thousand genes were subjected to IPA®, which demonstrated functional differences between treated and control groups. Relevant and significant ($P < 0.05$) 41 pathways induced by L-norvaline treatment and identified by IPA® are listed in accordance with their relative significance.

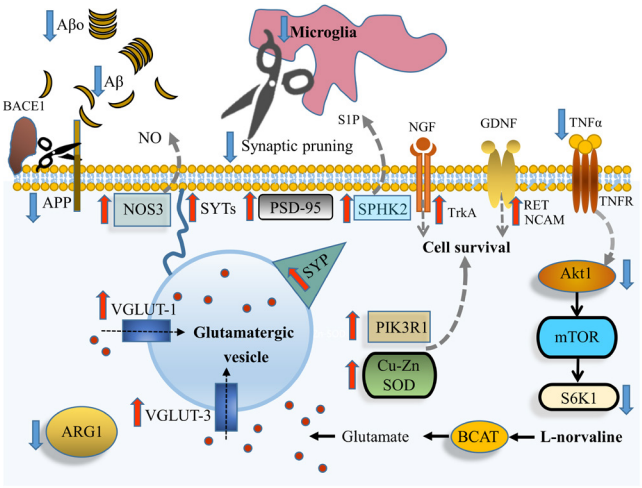

Figure 6 A proposed model for the metabolic effects of L-norvaline in the 3×Tg-AD mouse brain.
The treatment leads to reduced quantities of Aβ fibrils and prefibrillar oligomers (Aβo), which is caused by a decline in the levels of amyloid precursor protein (APP) but not beta-secretase 1 (BACE-1). L-Norvaline treatment reduces microglial density and shifts their phenotype from activated to resting, which, in turn, decreases the levels of tumor necrosis factor-α (TNFα), reduces synaptic pruning and increases spine density. L-Norvaline is a substrate of branched-chain amino acid aminotransferase (BCAT), which produces glutamate as the main product. The overproduction of glutamate leads to an increase in the expression levels of vesicular glutamate transporter 1 and 3 (VGLUT-1 and VGLUT-3, respectively), synaptophysin (SYP), synaptotagmins (SYTs). TNFα activates the mechanistic target of rapamycin (mTOR) pathway. L-Norvaline also reduces the levels of RAC-alpha protein-serine/threonine kinase (Akt1) and inhibits ribosomal protein S6 kinase beta-1 (S6K1). Nerve growth factor (NGF) binding to high affinity nerve growth factor receptor (TrkA) (which shows increased levels of expression in the L-Norvaline treated mice) causes the phosphorylation of TrkA and activation of multiple preventing apoptosis signaling pathways. Glial cell-derived neurotrophic factor (GDNF) binds to a multi-component receptor (GDNFRα1 and RET), which induces cell survival mechanisms. The levels of RET are escalated in the L-norvaline treated mice. Additionally, neural cell adhesion molecule (NCAM), (which is elevated by the treatment as well) serves as a second signaling receptor for GDNF. L-Norvaline increases the levels of sphingosine kinase 2 (SPHK2), which leads to an escalation of the neuroprotective factor sphingosine 1-phosphate (S1P) levels. Finally, L-norvaline increases the levels of superoxide dismutase [Cu-Zn] (SOD), and phosphatidylinositol 3-kinase regulatory subunit alpha (PIK3R1). Red arrows represent elevated levels, and blue arrows designate reduced levels compared to the vehicle-treated controls.

L-norvaline in a mouse model of AD. Previously we proved, by use of two canonical paradigms, that L-norvaline ameliorated short- and long-term memory deficits in the 3×Tg-AD mice, and demonstrated a significant reduction of Aβ-immunoreactivity in the cortices following the treatment (Polis et al., 2018). Here, we confirm these findings with another context-related memory test and report a significant reduction of the hippocampal Aβ burden.

To decipher the amyloidosis reduction mechanism, we performed western blotting of hippocampal lysates and studied the effects of L-norvaline treatment upon APP and BACE-1 expression. In the previous report, we revealed a substantial decrease in the levels of Aβ toxic oligomeric and fibrillary forms following the treatment. Here, we evidence a significant reduction of APP, but not BACE-1 protein levels. Therefore, we suggest that L-norvaline moderates the rate of APP translation, which leads to a dramatic decline in the hippocampal amounts of Aβ deposits and toxic oligomers.

Levels of soluble conformations of Aβ have been shown to correlate with AD-associated synaptic loss and cognitive impairment (McLean et al., 1999). Moreover, these species trigger neurotoxicity in the presence of microglia and potentiate proinflammatory changes in the AD brain (Dhawan et al., 2012). Current literature highlights chronic neuroinflammation as a prominent feature of AD pathogenesis (Heneka et al., 2015). Accordingly, there were attempts to interfere with inflammatory complement-mediated processes leading to the synaptic loss in AD mice.

The 3×Tg-AD mice exhibit a regional and age-dependent enhancement of F4/80-positive (Janelsins et al., 2005), IBA1-positive (Montgomery et al., 2011), and CD11b-positive microglia (Ye et al., 2016). The phenomenon is associated with amplification of various factors of inflammation in the brain, including TNFα (Montacute et al., 2017). Microglia and neurons typically express TNFα, and its expression intensifies in activated microglia and reactive astrocytes (Badoer, 2010). Fillit et al. disclosed meaningfully elevated levels of TNFα in the AD brains (Fillit et al., 1991). Animal

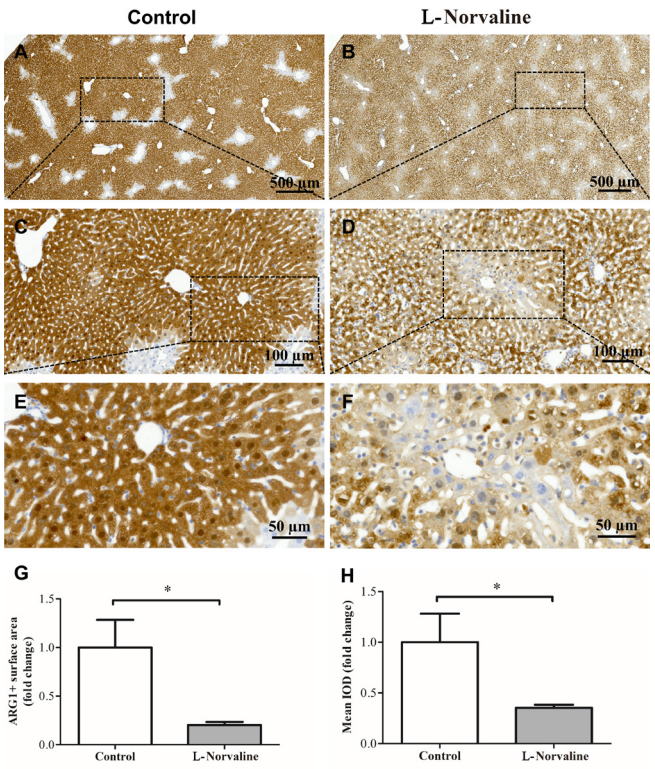

Figure 7 Immunohistochemical ARG1 staining of the 3×Tg-AD mouse liver tissue.
Bright-field ×40 micrographs of the liver from control (A, C, E) and L-Norvaline treated animals (B, D, F). The bar charts show a significant reduction in the ARG1$^+$ surface area (G) and integrated optical density (IOD) of ARG1$^+$ objects in the L-norvaline group (H). Data are presented as the mean ± SEM ($n = 8$ brain sections, four mice per group). $*P < 0.05$ (two-tailed Student's *t*-test).

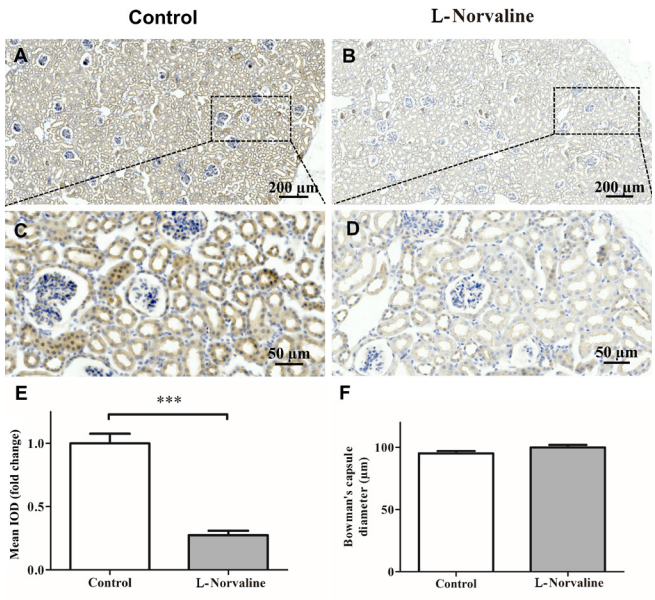

Figure 8 Immunohistochemical arginase 2 staining of the 3×Tg-AD mouse kidney tissue.
Representative ×20 bright-field micrographs of the longitudinally sliced kidneys from the control (A) and L-norvaline treated (B) mice. Insets (C, D) are ×40 images of outer medulla and cortex. The bar charts show a significant reduction in the integrated optical density (IOD) of arginase 2-immunoreactive objects in the L-norvaline group (E) ($n = 8$ brain sections, four mice per group). There was no significant effect on the Bowman's capsule diameter (F). Data are presented as the mean ± SEM ($n = 24$ cortical objects, three cortical objects per section, two sections per animal, four mice per group). $***P < 0.001$ (two-tailed Student's *t*-test).

studies confirm a link between excess TNFα levels in the brain and AD development (Janelsins et al., 2008; Cavanagh et al., 2016).

We previously demonstrated that L-norvaline treatment led to a decline in IBA1 immunoreactive cell' density in the hippocampi of 3×Tg-AD mice, which was associated with a shift from activated to resting ramified microglial phenotype (Polis et al., 2018). In the present study, we disclose a significant reduction in the hippocampal levels of TNFα mRNA expression following the treatment. It was convincingly demonstrated in primary cultures of mouse astrocytes that APP gene responds to the stimulation by TNFα (Lahiri et al., 2003). Remarkably, TNFα positively regulates APP transcription and translation *via* regulatory elements present in the APP promoter. Moreover, TNFα stimulates the expression levels of BACE1, which escalates the amyloidogenic APP processing (Zhao et al., 2011). Our findings also confirm the direct connection between TNFα and APP but not BACE-1 levels in the 3×Tg-AD mice.

There is a solidly grounded hypothesis that activated microglia cause synaptic and wiring dysfunction by pruning synaptic connections (Hong et al., 2016). Consequently, it was proposed to target the microglia-synapse pathways to prevent early AD symptoms (Xie et al., 2017). In the previous study, we reported a significant increase in dendritic spine density in the hippocampi of the L-norvaline treated mice. Here, we evidence an escalation of the PSD-95 protein levels in the hippocampi of the experimental group, which reflects the increase of spine density.

Accumulating empirical evidence suggests a role of mechanistic target of rapamycin (mTOR) in the regulation of immune responses (Powell et al., 2012) and major pathological processes of AD (Wang et al., 2014). Additionally, mTOR serves as a chief regulator of autophagy (Orr and Oddo, 2013), which is strongly associated with AD pathogenesis *via* its influence upon the endosomal-lysosomal function (Funderburk et al., 2010). Remarkably, rapamycin improves memory and effectively reduces amyloid and tau pathologies in the 3×Tg-AD mice (Caccamo et al., 2010). Accordingly, mTOR-signaling inhibition is a novel therapeutic target for AD (Tramutola et al., 2017). Recently, it was hypothesized and confirmed that mTOR affects TNF-mediated pro-inflammatory processes. Karonitsch et al. (2018) demonstrated in fibroblast culture that TNF activates the mTOR pathway, which, in turn, modulates the gene expression response to TNF.

L-norvaline possesses anti-inflammatory properties, which have been attributed to its potency of inhibiting ribosomal protein S6 kinase beta-1 (S6K1). This kinase is a downstream target of mTOR signaling (Ming et al., 2009). Previously we reported a significant reduction (by 53%) of RAC-alpha protein-serine/threonine kinase (Akt1) levels in the L-norvaline

treated mice (Polis et al., 2018). AKT1 is a key modulator of the AKT-mTOR-S6K1 signaling pathway that regulates various biological processes including metabolism, proliferation, and cell survival (Memmott and Dennis, 2009). TNF was shown to induce the activation of AKT and S6K1 (Karonitsch et al., 2018). Therefore, we speculate that the reduction in the levels of AKT1 protein following the L-norvaline treatment is TNFα-mediated (**Figure 6**). Of note, chronic rapamycin treatment does not modify the levels of TNFα in the brains of 3×Tg-AD mice (Majumder et al., 2011). Thus, the observed reduction in the TNFα gene expression levels following the treatment cannot be explained by L-norvaline modulation of the AKT-mTOR-S6K1 signaling pathway. Future investigations should address the elucidation of this phenomenon.

Our bioinformatics analysis revealed 41 critical biological processes involved in cell survival and immune response and significantly activated by L-norvaline treatment. The most significant pathways in the list are the neuregulin signaling pathway, synaptic long-term depression, ERK/MAPK signaling, PDGF signaling, and oncostatin M Signaling, which are essential for neuroprotection and their activation is particularly beneficial for AD patients.

L-norvaline is a potent non-competitive arginase inhibitor (Polis and Samson, 2018). Contemporary studies have identified arginase function in the brain and associated this enzyme with the development of neurodegenerative diseases (Patassini et al., 2015). Moreover, upregulation of arginase contributes to endothelial dysfunction, atherosclerosis, and diabetes. Therefore, regulation of arginase activity is an emerging universal approach for treatment of AD and other metabolic disorders.

Previous studies established the presence of both ARG1 and ARG2 in the brain (Peters et al., 2013; Polis et al., 2018). Moreover, arginase levels were shown to be increased in the areas with pronounced Aβ deposition (Kan et al., 2015; Polis et al., 2018). Of note, the primary metabolic function of arginases in mammals is the removal of excess ammonia *via* the urea cycle. This is the central role of ARG1 in the hepatic tissue (Stewart and Caron, 1977). ARG2 is a kidney-type arginase, which is ubiquitously expressed at a low level within the mitochondria of various organs (Lange et al., 2004).

Arginase inhibition with a potent reversible inhibitor of liver arginase N(omega)-hydroxy-nor-L-arginine (nor-NOHA) (Ki = 0.5 μM) ameliorates hepatic metabolism in obese mice (Moon et al., 2014). Of note, in the forementioned study, mice were orally gavaged with a relatively high dose of the arginase inhibitor (40 mg/kg per day) for 5 weeks. The authors conclude that arginase inhibition exerts protective properties against hepatic lipid abnormalities induced by obesity, and address arginase inhibition as a potential therapeutic approach for obesity and its metabolic complications. Another study, utilizing a several-fold higher (400–800 mg/kg) dose of nor-NOHA in rat demonstrated that arginase inhibition does not lead to changes in serum creatinine, alanine aminotransferase, alanine aminotransferase, or body weight in the animals. Moreover, histological analysis of liver, heart, lung, kidney, spleen, and pancreas did not reveal any structural abnormalities (Reid et al., 2007). Furthermore, even considerable reduction of the liver ARG1 activity (by 35%) does not affect general metabolic profile data in the rats (Sabbatini et al., 2003).

In this study, we aimed to investigate the influence of L-norvaline upon ARG1 and ARG2 levels in the primary organs of their expression. A set of the histochemical investigations revealed a significant reduction of ARG1 immunoreactivity in the liver and ARG2 immunoreactivity in the kidney following the treatment. It is worth mentioning that ARG2 deficiency extends the lifespan of mice (Xiong et al., 2017). Moreover, targeting ARG2 protects mice from high-fat-diet-induced hepatic steatosis through suppression of macrophage inflammation (Liu et al., 2016). Interestingly enough, the release of TNFα from bone marrow-derived macrophages of $Arg2^{-/-}$ mice is decreased as compared to the WT animals. Therefore, strong inhibition of ARG2 levels by L-norvaline might be beneficial for the experimental mice.

Previously we have proved that L-norvaline treatment does not lead to a significant drop in weight or detectable changes in the behavior of the WT mice (Polis et al., 2018). Moreover, the treatment does not affect the levels of ARG1 and ARG2 expression in their brains. Nevertheless, L-norvaline reduces amyloid-beta-driven arginase immunoreactivity in the aged 3×Tg-AD animals. For that reason, we suggest that arginase inhibition with L-norvaline provides a fine-tuning of the enzyme activity, primarily in the organs where some pathological stimuli upregulate it.

In conclusion, we emphasize that arginase inhibition, in general, shows a wide-ranging therapeutic potential for the treatment of various pathologies. In this context, we underline multifaceted modes of L-norvaline activity, which interfere with several critical aspects of AD pathogenesis. Therefore, the substance represents a promising neuroprotective agent that deserves to be clinically investigated.

Acknowledgments: *We gratefully acknowledge Dr. Zohar Gavish for his help with immunohistochemistry and Dr. Tali Shalit for her help with bioinformatics analysis.*
Author contributions: *Study design: BP, AOS; experiment implementation and data analysis: BP; western blotting: KDS; RT-PCR: VG; experiment advising and supervising: HGH; manuscript writing: BP; manuscript editing: AOS and HGH. All authors approved the final version of this paper.*
Conflicts of interest: *None declared.*
Financial support: *This research was supported by Marie Curie CIG Grant 322113, Leir Foundation Grant, Ginzburg Family Foundation Grant, and Katz Foundation Grant (all to AOS). Funders had no involvement in the study design; data collection, analysis, and interpretation; paper writing; or decision to submit the paper for publication.*
Institutional review board statement: *The study was approved by the Bar-Ilan University Animal Care and Use Committee (approval No. 82-10-2017) on October 1, 2017.*

Data sharing statement: *Datasets analyzed during the current study are available from the corresponding author on reasonable request.*
Plagiarism check: *Checked twice by iThenticate.*
Peer review: *Externally peer reviewed.*

Additional file:

Additional Table 1: Kinex™ antibody microarray data report.

References

Airaksinen MS, Saarma M (2002) The GDNF family: Signalling, biological functions and therapeutic value. Nat Rev Neurosci 3:383-394.

Allen SJ, Watson JJ, Shoemark DK, Barua NU, Patel NK (2013) GDNF, NGF and BDNF as therapeutic options for neurodegeneration. Pharmacol Ther 138:155-175

Anagnostaras SG, Gale GD, Fanselow MS (2001) Hippocampus and contextual fear conditioning: Recent controversies and advances. Hippocampus 11:8-17.

Badoer E (2010) Microglia: activation in acute and chronic inflammatory states and in response to cardiovascular dysfunction. Int J Biochem Cell Biol 42:1580-1585.

Bevilaqua LR, Rossato JI, Medina JH, Izquierdo I, Cammarota M (2003) Src kinase activity is required for avoidance memory formation and recall. Behav Pharmacol 14:649-652.

Caccamo A, Majumder S, Richardson A, Strong R, Oddo S (2010) Molecular interplay between mammalian target of rapamycin (mTOR), amyloid-beta, and Tau: effects on cognitive impairments. J Biol Chem 285:13107-13120.

Cavanagh C, Tse YC, Nguyen HB, Krantic S, Breitner JCS, Quirion R, Wong TP (2016) Inhibiting tumor necrosis factor-α before amyloidosis prevents synaptic deficits in an Alzheimer's disease model. Neurobiol Aging 47:41-49.

Chang R, Yee KL, Sumbria RK (2017) Tumor necrosis factor α Inhibition for Alzheimer's Disease. J Cent Nerv Syst Dis 9: 1179573517709278.

Couttas TA, Kain N, Daniels B, Lim XY, Shepherd C, Kril J, Pickford R, Li H, Garner B, Don AS (2014) Loss of the neuroprotective factor Sphingosine 1-phosphate early in Alzheimer's disease pathogenesis. Acta Neuropathol Commun 2:9.

Croft CL, Wade MA, Kurbatskaya K, Mastrandreas P, Hughes MM, Phillips EC, Pooler AM, Perkinton MS, Hanger DP, Noble W (2017) Membrane association and release of wild-type and pathological tau from organotypic brain slice cultures. Cell Death Dis 8:e2671.

Dhawan G, Floden AM, Combs CK (2012) Amyloid-β oligomers stimulate microglia through a tyrosine kinase dependent mechanism. Neurobiol Aging 33:2247-2261.

Dominguez G, Maddelein M-L, Pucelle M, Nicaise Y, Maurage C-A, Duyckaerts C, Cuvillier O, Delisle M-B (2018) Neuronal sphingosine kinase 2 subcellular localization is altered in Alzheimer's disease brain. Acta Neuropathol Commun 6:25.

Doody RS, Raman R, Farlow M, Iwatsubo T, Vellas B, Joffe S, Kieburtz K, He F, Sun X, Thomas RG, Aisen PS, Siemers E, Sethuraman G, Mohs R (2013) A phase 3 trial of semagacestat for treatment of Alzheimer's disease. N Engl J Med 369:341-350.

Drinkut A, Tillack K, Meka DP, Schulz JB, Kügler S, Kramer ER (2016) Ret is essential to mediate GDNF's neuroprotective and neuroregenerative effect in a Parkinson disease mouse model. Cell Death Dis 7:e2359.

Eyjolfsdottir H, Eriksdotter M, Linderoth B, Lind G, Juliusson B, Kusk P, Almkvist O, Andreasen N, Blennow K, Ferreira D, Westman E, Nennesmo I, Karami A, Darreh-Shori T, Kadir A, Nordberg A, Sundström E, Wahlund LO, Wall A, Wiberg M, et al. (2016) Targeted delivery of nerve growth factor to the cholinergic basal forebrain of Alzheimer's disease patients: application of a second-generation encapsulated cell biodelivery device. Alzheimers Res Ther 8:30.

Fillit H, Ding W, Buee L, Kalman J, Altstiel L, Lawlor B, Wolf-Klein G (1991) Elevated circulating tumor necrosis factor levels in Alzheimer's disease. Neurosci Lett 129:318-320.

Franklin KBJ, Paxinos G (2007) The Mouse Brain in Stereotaxic Coordinates. 3rd ed. San Diego, CA, USA: Academic Press.

Funa K, Sasahara M (2014) The roles of PDGF in development and during neurogenesis in the normal and diseased nervous system. J Neuroimmune Pharmacol 9:168-181.

Funderburk SF, Marcellino BK, Yue Z (2010) Cell "self-eating" (autophagy) mechanism in Alzheimer's disease. Mt Sinai J Med 77:59-68.

Furigo IC, Melo HM, Lyra e Silva NM, Ramos-Lobo AM, Teixeira PDS, Buonfiglio DC, Wasinski F, Lima ER, Higuti E, Peroni CN, Bartolini P, Soares CRJ, Metzger M, de Felice FG, Donato J (2018) Brain STAT5 signaling modulates learning and memory formation. Brain Struct Funct 223:2229-2241

Gueli MC, Taibi G (2013) Alzheimer's disease: Amino acid levels and brain metabolic status. Neurol Sci 34:1575-1579.

Heneka MT, Carson MJ, El Khoury J, Landreth GE, Brosseron F, Feinstein DL, Jacobs AH, Wyss-Coray T, Vitorica J, Ransohoff RM, Herrup K, Frautschy SA, Finsen B, Brown GC, Verkhratsky A, Yamanaka K, Koistinaho J, Latz E, Halle A, Petzold GC, et al. (2015) Neuroinflammation in Alzheimer's disease. Lancet Neurol 14:388-405.

Hla T, Brinkmann V (2011) Sphingosine 1-phosphate (S1P): Physiology and the effects of S1P receptor modulation. Neurology 76(8 Suppl 3):S3-8.

Hohman TJ, Bell SP, Jefferson AL (2015) The role of vascular endothelial growth factor in neurodegeneration and cognitive decline: exploring interactions with biomarkers of Alzheimer's disease. JAMA Neurol 72:520-529.

Hong S, Dissing-Olesen L, Stevens B (2016) New insights on the role of microglia in synaptic pruning in health and disease. Curr Opin Neurobiol 36:128-134.

Iulita MF, Cuello AC (2014) Nerve growth factor metabolic dysfunction in Alzheimer's disease and Down syndrome. Trends Pharmacol Sci 35:338-348.

Janelsins MC, Mastrangelo MA, Oddo S, LaFerla FM, Federoff HJ, Bowers WJ (2005) Early correlation of microglial activation with enhanced tumor necrosis factor-alpha and monocyte chemoattractant protein-1 expression specifically within the entorhinal cortex of triple transgenic Alzheimer's disease mice. J Neuroinflammation 2:23.

Janelsins MC, Mastrangelo MA, Park KM, Sudol KL, Narrow WC, Oddo S, LaFerla FM, Callahan LM, Federoff HJ, Bowers WJ (2008) Chronic neuron-specific tumor necrosis factor-alpha expression enhances the local inflammatory environment ultimately leading to neuronal death in 3xTg-AD mice. Am J Pathol 173:1768-1782.

Kan MJ, Lee JE, Wilson JG, Everhart AL, Brown CM, Hoofnagle AN, Jansen M, Vitek MP, Gunn MD, Colton CA (2015) Arginine Deprivation and Immune Suppression in a Mouse Model of Alzheimer's Disease. J Neurosci 35:5969-5982.

Karmarkar SW, Bottum KM, Krager SL, Tischkau SA (2011) ERK/MAPK is essential for endogenous neuroprotection in scn2.2 cells. PLoS One 6:e23493.

Karonitsch T, Kandasamy RK, Kartnig F, Herdy B, Dalwigk K, Niederreiter B, Holinka J, Sevelda F, Windhager R, Bilban M, Weichhart T, Säemann M, Pap T, Steiner G, Smolen JS, Kiener HP, Superti-Furga G (2018) mTOR senses environmental cues to shape the fibroblast-like synoviocyte response to inflammation. Cell Rep 23:2157-2167.

Lahiri DK, Chen D, Vivien D, Ge YW, Greig NH, Rogers JT (2003) Role of cytokines in the gene expression of amyloid β-protein precursor: Identification of a 5′ -UTR-binding nuclear factor and its implications in Alzheimer's disease. J Alzheimer's Dis 5:81-90.

Lahiri DK, Maloney B, Long JM, Greig NH (2014) Lessons from a BACE1 inhibitor trial: Off-site but not off base. Alzheimers Dement 10(5 Suppl):S411-419.

Lange PS, Langley B, Lu P, Ratan RR (2004) Novel roles for arginase in cell survival, regeneration, and translation in the central nervous system. J Nutr 134:2812S-2819S.

Liu C, Rajapakse AG, Riedo E, Fellay B, Bernhard MC, Montani JP, Yang Z, Ming XF (2016) Targeting arginase-II protects mice from high-fat-diet-induced hepatic steatosis through suppression of macrophage inflammation. Sci Rep 6:20405.

Liu P, Fleete MS, Jing Y, Collie ND, Curtis MA, Waldvogel HJ, Faull RL, Abraham WC, Zhang H (2014) Altered arginine metabolism in Alzheimer's disease brains. Neurobiol Aging 35:1992-2003.

Livak KJ, Schmittgen TD (2001) Analysis of relative gene expression data using real-time quantitative PCR and the 2-ΔΔCT method. Methods 25:402-408.

Lüthi A, Laurent JP, Figurovt A, Mullert D, Schachnert M (1994) Hippocampal long-term potentiation and neural cell adhesion molecules L1 and NCAM. Nature 372:777-779.

Majumder S, Richardson A, Strong R, Oddo S (2011) Inducing autophagy by rapamycin before, but not after, the formation of plaques and tangles ameliorates cognitive deficits. PLoS One 6:e25416.

McLean CA, Cherny RA, Fraser FW, Fuller SJ, Smith MJ, Beyreuther K, Bush AI, Masters CL (1999) Soluble pool of Aβ amyloid as a determinant of severity of neurodegeneration in Alzheimer's disease. Ann Neurol 46:860-866.

Mei L, Nave KA (2014) Neuregulin-ERBB signaling in the nervous system and neuropsychiatric diseases. Neuron 83:27-49.
Memmott RM, Dennis PA (2009) Akt-dependent and -independent mechanisms of mTOR regulation in cancer. Cell Signal 21:656-664.
Ming XF, Rajapakse AG, Carvas JM, Ruffieux J, Yang Z (2009) Inhibition of S6K1 accounts partially for the anti-inflammatory effects of the arginase inhibitor L-norvaline. BMC Cardiovasc Disord 9:12.
Miyanaka K, Gotoh T, Nagasaki A, Takeya M, Ozaki M, Iwase K, Takiguchi M, Iyama KI, Tomita K, Mori M (1998) Immunohistochemical localization of arginase II and other enzymes of arginine metabolism in rat kidney and liver. Histochem J 30:741-751.
Montacute R, Foley K, Forman R, Else KJ, Cruickshank SM, Allan SMR (2017) Enhanced susceptibility of triple transgenic Alzheimer's disease (3xTg-AD) mice to acute infection. J Neuroinflammation 14:50.
Montgomery SL, Mastrangelo MA, Habib D, Narrow WC, Knowlden SA, Wright TW, Bowers WJ (2011) Ablation of TNF-RI/RII expression in Alzheimer's disease mice leads to an unexpected enhancement of pathology: Implications for chronic pan-TNF-α suppressive therapeutic strategies in the brain. Am J Pathol 179:2053-2070.
Moon J, Do HJ, Cho Y, Shin MJ (2014) Arginase inhibition ameliorates hepatic metabolic abnormalities in obese mice. PLoS One 9:e103048.
Mori F, Rossi S, Piccinin S, Motta C, Mango D, Kusayanagi H, Bergami A, Studer V, Nicoletti CG, Buttari F, Barbieri F, Mercuri NB, Martino G, Furlan R, Nistico R, Centonze D (2013) Synaptic Plasticity and PDGF Signaling Defects Underlie Clinical Progression in Multiple Sclerosis. J Neurosci 33:19112-19119.
Morris GP, Clark IA, Zinn R, Vissel B (2013) Microglia: A new frontier for synaptic plasticity, learning and memory, and neurodegenerative disease research. Neurobiol Learn Mem 105:40-53.
Nguyen TLX, Kim CK, Cho JH, Lee KH, Ahn JY (2010) Neuroprotection signaling pathway of nerve growth factor and brain-derived neurotrophic factor against staurosporine induced apoptosis in hippocampal H19-7 cells. Exp Mol Med 42:583-595.
Oddo S, Caccamo A, Shepherd JD, Murphy MP, Golde TE, Kayed R, Metherate R, Mattson MP, Akbari Y, LaFerla FM (2003) Triple-transgenic model of Alzheimer's Disease with plaques and tangles: Intracellular Aβ and synaptic dysfunction. Neuron 39:409-421.
Orr ME, Oddo S (2013) Autophagic/lysosomal dysfunction in Alzheimer's disease. Alzheimer's Res Ther 5:53.
Osborn LM, Kamphuis W, Wadman WJ, Hol EM (2016) Astrogliosis: An integral player in the pathogenesis of Alzheimer's disease. Prog Neurobiol 144:121-141.
Paratcha G, Ledda F, Ibáñez CF (2003) The neural cell adhesion molecule NCAM is an alternative signaling receptor for GDNF family ligands. Cell 113:867-879.
Parikh V, Howe WM, Welchko RM, Naughton SX, D'Amore DE, Han DH, Deo M, Turner DL, Sarter M (2013) Diminished trkA receptor signaling reveals cholinergic-attentional vulnerability of aging. Eur J Neurosci 37:278-293.
Patassini S, Begley P, Reid SJ, Xu J, Church SJ, Curtis M, Dragunow M, Waldvogel HJ, Unwin RD, Snell RG, Faull RLM, Cooper GJS (2015) Identification of elevated urea as a severe, ubiquitous metabolic defect in the brain of patients with Huntington's disease. Biochem Biophys Res Commun 468:161-166.
Peluffo H, Acarin L, Arís A, González P, Villaverde A, Castellano B, González B (2006) Neuroprotection from NMDA excitotoxic lesion by Cu/Zn superoxide dismutase gene delivery to the postnatal rat brain by a modular protein vector. BMC Neurosci 7:1-11.
Peng S, Wuu J, Mufson EJ, Fahnestock M (2005) Precursor form of brain-derived neurotrophic factor and mature brain-derived neurotrophic factor are decreased in the pre-clinical stages of Alzheimer's disease. J Neurochem 93:1412-1421.
Peters D, Berger J, Langnaese K, Derst C, Madai VI, Krauss M, Fischer KD, Veh RW, Laube G (2013) Arginase and arginine decarboxylase - Where do the putative gate keepers of polyamine synthesis reside in rat brain? PLoS One 8:e66735.
Polis B, Samson AO (2018) Arginase as a potential target in the treatment of Alzheimer's disease. Adv Alzheimer's Dis 07:119-140.
Polis B, Srikanth KD, Elliott E, Gil-Henn H, Samson AO (2018) L-Norvaline reverses cognitive decline and synaptic loss in a murine model of Alzheimer's disease. Neurotherapeutics 15:1036-1054.
Powell JD, Pollizzi KN, Heikamp EB, Horton MR (2012) Regulation of immune responses by mTOR. Annu Rev Immunol 30:39-68.
Reid KM, Tsung A, Kaizu T, Jeyabalan G, Ikeda A, Shao L, Wu G, Murase N, Geller DA (2007) Liver I/R injury is improved by the arginase inhibitor, N(omega)-hydroxy-nor-L-arginine (nor-NOHA). Am J Physiol Liver Physiol 292:G512-517.
Revilla S, Suñol C, García-Mesa Y, Giménez-Llort L, Sanfeliu C, Cristòfol R (2014a) Physical exercise improves synaptic dysfunction and recovers the loss of survival factors in 3xTg-AD mouse brain. Neuropharmacology 81:55-63.
Revilla S, Ursulet S, Álvarez-López MJ, Castro-Freire M, Perpiñá U, García-Mesa Y, Bortolozzi A, Giménez-Llort L, Kaliman P, Cristòfol R, Sarkis C, Sanfeliu C (2014b) Lenti-GDNF gene therapy protects against Alzheimer's disease-like neuropathology in 3xTg-AD mice and MC65 cells. CNS Neurosci Ther 20:961-972.
Rosenstein JM, Krum JM, Ruhrberg C (2010) VEGF in the nervous system. Organogenesis 6:107-114.
Sabbatini M, Pisani A, Uccello F, Fuiano G, Alfieri R, Cesaro A, Cianciaruso B, Andreucci VE (2003) Arginase inhibition slows the progression of renal failure in rats with renal ablation. Am J Physiol Physiol 284:F680-687.
Schaeffer EL, Figueiró M, Wagner I, Gattaz F (2011) Insights into Alzheimer disease pathogenesis from studies in transgenic animal models. Clinics 66:45-54.
Selkoe DJ, Hardy J (2002) The amyloid hypothesis of Alzheimer's disease: Progress and problems on the road to therapeutics. Science 297:353-356.
Sly LM, Krzesicki RF, Brashler JR, Buhl AE, McKinley DD, Carter DB, Chin JE (2001) Endogenous brain cytokine mRNA and inflammatory responses to lipopolysaccharide are elevated in the Tg2576 transgenic mouse model of Alzheimer's disease. Brain Res Bull 56:581-588.
Spangenberg EE, Lee RJ, Najafi AR, Rice RA, Elmore MRP, Blurton-Jones M, West BL, Green KN (2016) Eliminating microglia in Alzheimer's mice prevents neuronal loss without modulating amyloid-β pathology. Brain 139:1265-1281.
Stewart J, Caron H (1977) Arginases of mouse brain and liver. J Neurochem 29:657-663.
Szatmari E, Kalita KB, Kharebava G, Hetman M (2007) Role of kinase suppressor of Ras-1 in neuronal survival signaling by extracellular signal-regulated kinase 1/2. J Neurosci 27:11389-11400.
Thakur V, Morse S, Reisin E (2006) Functional and structural renal changes in the early stages of obesity. Contrib Nephrol 151:135-150.
Tobar A, Ori Y, Benchetrit S, Milo G, Herman-Edelstein M, Zingerman B, Lev N, Gafter U, Chagnac A (2013) Proximal tubular hypertrophy and enlarged glomerular and proximal tubular urinary space in obese subjects with proteinuria. PLoS One 8:e75547.
Tramutola A, Lanzillotta C, Di Domenico F (2017) Targeting mTOR to reduce Alzheimer-related cognitive decline: from current hits to future therapies. Expert Rev Neurother 17:33-45.
Wang C, Yu JT, Miao D, Wu ZC, Tan M-S, Tan L (2014) Targeting the mTOR signaling network for Alzheimer's disease therapy. Mol Neurobiol 49:120-135.
Wehner JM, Radcliffe RA (2004) Cued and contextual fear conditioning in mice. Curr Protoc Neurosci Chapter 8:Unit 8.5C.
Xie J, Wang H, Lin T, Bi B (2017) Microglia-synapse pathways: Promising therapeutic strategy for Alzheimer's disease. Biomed Res Int 2017.
Xiong Y, Yepuri G, Montani JP, Ming XF, Yang Z (2017) Arginase-II deficiency extends lifespan in mice. Front Physiol 8:682.
Xu J, Begley P, Church SJ, Patassini S, Hollywood KA, Jüllig M, Curtis MA, Waldvogel HJ, Faull RLM, Unwin RD, Cooper GJ (2016a) Graded perturbations of metabolism in multiple regions of human brain in Alzheimer's disease: Snapshot of a pervasive metabolic disorder. Biochim Biophys Acta 1862:1084-1092.
Xu J, De Winter F, Farrokhi C, Rockenstein E, Mante M, Adame A, Cook J, Jin X, Masliah E, Lee KF (2016b) Neuregulin 1 improves cognitive deficits and neuropathology in an Alzheimer's disease model. Sci Rep 6:31692.
Ye M, Chung H-S, Lee C, Yoon MS, Yu AR, Kim JS, Hwang D-S, Shim I, Bae H (2016) Neuroprotective effects of bee venom phospholipase A2 in the 3xTg AD mouse model of Alzheimer's disease. J Neuroinflammation 13:10.
Yu X, Rajala RVS, McGinnis JF, Li F, Anderson RE, Yan X, Li S, Elias R V., Knapp RR, Zhou X, Cao W (2004) Involvement of Insulin/Phosphoinositide 3-Kinase/Akt Signal Pathway in 17β-Estradiol-mediated Neuroprotection. J Biol Chem 279:13086-13094.
Zhang F, Wang S, Cao G, Gao Y, Chen J (2007) Signal transducers and activators of transcription 5 contributes to erythropoietin-mediated neuroprotection against hippocampal neuronal death after transient global cerebral ischemia. Neurobiol Dis 25:45-53.
Zhao J, O'Connor T, Vassar R (2011) The contribution of activated astrocytes to Aβ production: Implications for Alzheimer's disease pathogenesis. J Neuroinflammation 8:150.

C-Editors: Zhao M, Li CH; T-Editor: Liu XL

Additional Table 1 Kinex™ antibody microarray data report

No	Target name with alias	Full target protein name	%CFC	*P*-value
1	SCNN1B	Amiloride-sensitive sodium channel subunit beta	220	0.018
2	Src	Src proto-oncogene-encoded protein-tyrosine kinase	94	0.003
3	MYPT1	Protein phosphatase 1 regulatory subunit 12A	94	0.009
4	PP2A B	Protein-serine phosphatase 2A - B regulatory subunit - B56 alpha isoform	92	0.032
5	NPM1 (B23)	Nucleophosmin	87	0.007
6	MEK1 (MAP2K1; MKK1)	MAPK/ERK dual-specificity kinase 1	86	0.015
7	PKCb (PRKCB1)	Protein-serine kinase C beta 1	85	0.017
8	PLCG1	1-phosphatidylinositol 4,5-bisphosphate phosphodiesterase gamma-1	84	0.030
9	Bcr	Breakpoint cluster region protein	80	0.043
10	Ros (ROS1)	Orosomucoid 1 receptor-tyrosine kinase	78	0.003
11	PHOCN (MOB4; mMOB1)	MOB-like protein phocein (Preimplantation protein 3)	76	0.038
12	STAT1a	Signal transducer and activator of transcription 1 alpha	74	0.014
13	ELK1	ETS domain-containing protein Elk-1	72	0.032
14	VGLUT3	Vesicular glutamate transporter 3	71	0.012
15	eNos (NOS3)	Nitric oxide synthase, endothelial	68	0.041
16	Rad17	Cell cycle checkpoint protein RAD17	67	0.003
17	Ksr1	Protein-serine kinase suppressor of Ras 1	59	0.036
18	TrkA (NGFR; NTRK1)	Nerve growth factor (NGF) receptor-tyrosine kinase	56	0.039
19	SPHK2	Sphingosine kinase 2	56	0.036
20	PKG1a (PRKG1A)	cGMP-dependent protein kinase I-alpha	54	0.003
21	Cyclin E1 (CCNE1)	Cyclin E1	54	0.015
22	Ret (c-Ret; GDNF receptor; Glial cell line-derived neurotropic factor receptor)	Proto-oncogene tyrosine-protein kinase receptor Ret	53	0.040
23	Tlk1	Tousled-like protein-serine kinase 1	53	0.029
24	Synaptophysin	Synaptophysin	50	0.039

25	CaMKK (CaMKK1)	Calcium-calmodulin-dependent protein kinase kinase 1	50	0.026
26	Haspin	Protein-serine/threonine kinase haspin	49	0.033
27	PKCa (PRKCA)	Protein-serine kinase C alpha	49	0.013
28	MyoD (MYOD1)	Myoblast determination protein 1	47	0.035
29	MEK1 (MAP2K1; MKK1)	MAPK/ERK dual-specificity kinase 1	46	0.001
30	Mnk2 (MKNK2)	MAP kinase-interacting serine-threonine kinase 2	45	0.040
31	STAT5A	Signal transducer and activator of transcription 5A	45	0.006
32	NrCAM	Neuronal cell adhesion molecule	43	0.003
33	INPP5F (OCRL)	Inositol polyphosphate 5-phosphatase OCRL-1	43	0.022
34	PKAR2B	cAMP-dependent protein-serine kinase regulatory type 2 subunit beta	43	0.038
35	MRCKb	Protein-serine/threonine kinase MRCK beta	42	0.001
36	Mos	Moloney sarcoma oncogene-encoded protein-serine kinase	42	0.012
37	TNFR1 (CD120a; TNFRSF1A; TNFAR)	Tumour necrosis factor receptor superfamily member 1A	42	0.022
38	ACTA1 (Alpha-actin)	Actin, alpha, beta and gamma	41	0.009
39	Paxillin 1 (PXN)	Paxillin 1	41	0.034
40	TEC	Protein-tyrosine kinase Tec	40	0.034
41	Nrf2 (NFE2L2)	Nuclear factor erythroid 2-related factor 2	40	0.020
42	Beclin 1 (BECN1; GT197)	Beclin-1	40	0.045
43	PP2A/Bb (PPP2R2B)	Protein-serine phosphatase 2A - B regulatory subunit - beta isoform	39	0.016

44	CavBeta2 (CACNB2; CAB2)	Voltage-dependent L-type calcium channel subunit beta-2	38	0.038
45	ACACA (ACC1; ACCA)	Acetyl-CoA carboxylase 1	37	0.032
46	DAB1	Disabled homologue 1	37	0.015
47	ACTA1 (Alpha-actin)	Actin, alpha skeletal muscle	35	0.049
48	Raf1 (c-Raf)	RAF proto-oncogene serine/threonine-protein kinase	34	0.030
49	Src	Src proto-oncogene-encoded protein-tyrosine kinase	34	0.006
50	BLNK	B-cell linker protein	33	0.045
51	SYT10	Synaptotagmin-10	33	0.010
52	STAT5B	Signal transducer and activator of transcription 5B	32	0.019
53	OSR1	Protein odd-skipped-related 1	32	0.034
54	Kit	Mast/stem cell growth factor receptor Kit	31	0.029
55	COX4I1	Cytochrome c oxidase subunit 4 isoform 1, mitochondrial	31	0.024
56	PKCb2 (PRKCB2)	Protein-serine kinase C beta 2	30	0.047
57	PKCb (PRKCB1)	Protein-serine kinase C beta 1	29	0.041
58	MOK	MAPK/MAK/MRK overlapping kinase	29	0.040
59	PKR1 (PRKR; EIF2AK2)	Double stranded RNA dependent protein-serine kinase	29	0.039
60	RAB5A (Rab5)	Ras-related protein Rab-5A	29	0.018
61	HSP105 (HSPH1, HSP110)	Heat shock 105 kDa protein	29	0.032
62	CaMK1a (CaMKI)	Calcium/calmodulin-dependent protein-serine kinase 1 alpha	29	0.003
63	MEK2 (MAP2K2; MKK2)	MAPK/ERK dual-specificity kinase 2	29	0.037
64	EphA1	Ephrin type-A receptor 1 protein-tyrosine kinase	28	0.041
65	CaMK1a (CaMKI)	Calcium/calmodulin-dependent protein-serine kinase 1 alpha	28	0.043
66	MKK3 (MAP2K3; MEK3)	MAPK/ERK dual-specificity kinase 3 beta isoform	28	0.003
67	PAK3 (PAKb)	p21-activated kinase 3 (beta) (Protein-serine/threonine kinase PAK3)	27	0.046
68	Cyclin D1 (CCND1)	Cyclin D1	25	0.031
69	JAK3	Janus protein-tyrosine kinase 3	25	0.030
70	PP2A/Ca (PPP2CA)/'PP2A/Cb	Protein-serine phosphatase 2A - catalytic subunit - alpha and beta isoform	24	0.022

	(PPP2CB)			
71	PP2B-B1/2	Calcineurin subunit B type 2	24	0.005
72	PIK3R1 (PI3K p85)	Phosphatidylinositol 3-kinase regulatory subunit alpha	24	0.034
73	Synapsin 1	Synapsin 1 isoform Ia	24	0.009
74	RSK4 (RPS6KA6)	Ribosomal S6 protein-serine kinase 4 (alpha 6)	24	0.001
75	ITGA4 (CD49D)	Integrin alpha 4 (VLA4)	23	0.044
76	KRAS (KRAS2)	GTPase KRas	23	0.002
77	AMPKa1	5'-AMP-activated protein kinase catalytic subunit alpha-1	22	0.035
78	Pim2	Protein-serine/threonine kinase pim-2	22	0.003
79	DICER1	Endoribonuclease Dicer	21	0.028
80	p38d MAPK (MAPK13)	Mitogen-activated protein-serine kinase p38 delta	20	0.023
81	VEGFR1 (Flt1)	Vascular endothelial growth factor receptor 1	20	0.026
82	LAR (PTPRF)	Receptor-type tyrosine-protein phosphatase F	20	0.002
83	WNK2 (PRKWNK2)	Protein-serine/threonine kinase WNK2	20	0.026
84	ATM	Ataxia telangiectasia mutated	20	0.011
85	SOD3	Extracellular superoxide dismutase [Cu-Zn]	19	0.041
86	CDK10	Cyclin-dependent protein-serine kinase 10	19	0.019
87	TRRAP	Transformation/transcription domain-associated protein	18	0.037
88	PUMA (CHST9)	Carbohydrate sulfotransferase 9	18	0.048
89	MRCKa	Protein-serine/threonine kinase MRCK alpha	18	0.018

90	GSK3 Beta (GSK3b)	Glycogen synthase kinase-3 beta	18	0.017
91	BCL2A1	Bcl-2-related protein A1	17	0.049
92	PP1/Ca (PPP1CA)	Protein-serine phosphatase 1 - catalytic subunit - alpha isoform	17	0.009
93	TLR4 (CD284)	Toll-like receptor 4	17	0.037
94	JNK3 (SAPKb)	Jun N-terminus protein-serine kinase 3 (Stress-activated protein kinase-beta)	16	0.036
95	SLC38A1 (ATA1; NAT2)	Sodium-coupled neutral amino acid transporter 1	16	0.049
96	SYT6	Synaptotagmin-6	16	0.014
97	ATG4B	Cysteine protease, Autophagy-related protein ATG4B	15	0.032
98	CDKL3	Cyclin-dependent kinase-like 3	15	0.044
99	VEGFR2 (KDR, Flk1)	Vascular endothelial growth factor receptor-tyrosine kinase 2	14	0.028
100	Malin (NHLRC1; EPM2B)	E3 ubiquitin-protein ligase NHLRC1	14	0.033
101	JNK1 (MAPK8; SAPK1)	Jun N-terminus protein-serine kinase (Stress-activated protein kinase) 1	14	0.000
102	PKCm (PRKCM, PRKD1, PKD1)	Protein-serine kinase C mu (Protein kinase D)	14	0.039
103	MKK3 (MAP2K3; MEK3)	MAPK/ERK dual-specificity kinase 3 beta isoform	14	0.037
104	SRPK2	Serine/arginine-rich protein-specific kinase 2 (SRSF protein kinase 2)	13	0.007
105	JAK1	Janus protein-tyrosine kinase 1	13	0.013
106	SYT10	Synaptotagmin-12	12	0.032
107	SGK1	Protein-serine/threonine kinase Sgk1	11	0.028
108	Caveolin 2	Caveolin 2	11	0.038
109	PP2A/Bb (PPP2R2B)	Protein-serine phosphatase 2A - B regulatory subunit - beta isoform	10	0.010
110	AurKA (Aurora A, AIK)	Aurora Kinase A (Protein-serine/threonine kinase 6)	10	0.021
111	CD45	Receptor protein-tyrosine phosphatase CD45	9	0.042
112	TAK1 (MAP3K7)	TGF-beta-activated protein-serine kinase 1	9	0.018
113	PDK1 (PDHK1)	[Pyruvate dehydrogenase [lipoamide]] kinase isozyme 1, mitochondrial	8	0.017
114	ULK4	Unc-51-like protein-serine/threonine kinase 4	3	0.005
115	p38g MAPK	Mitogen-activated protein-serine kinase p38	-10	0.015

	(MAPK12, ERK6, SAPK3)	gamma		
116	CK1e (CSNK1E)	Casein protein-serine kinase 1 epsilon	-10	0.027
117	SCN3B (NaVbeta3)	Sodium channel subunit beta-3	-11	0.041
118	PTGES3 (p23)	Prostaglandin E synthase 3	-13	0.005
119	A-Raf	Protein-serine/threonine kinase A-Raf	-15	0.031
120	Nek2	NIMA (never-in-mitosis)-related protein-serine kinase 2	-16	0.025
121	Striatin	Striatin	-22	0.015
122	HO1 (HO; HMOX1)	Heme oxygenase 1	-24	0.005
123	REEP1	Receptor expression-enhancing protein 1	-25	0.049
124	Plk4 (SAK; STK18)	Polo-like protein-serine kinase 4	-25	0.004
125	DUSP7	Dual specificity protein phosphatase-7	-25	0.003
126	HSP72	Heat shock-related 70 kDa protein 2	-27	0.024
127	HSP90AB1 (HSP90; HSP84; HSP90B; HSPC2; HSPCB)	Heat shock 90 kDa protein beta	-35	0.045
128	PP2A B (PPP2R5A; B56)	Protein-serine phosphatase 2A - B regulatory subunit - B56 alpha isoform	-36	0.008
129	CDK5	Cyclin-dependent protein-serine kinase 5	-36	0.024
130	PDI (P4hb; PDIA1; ERBA2L; PO4DB)	Protein disulfide-isomerase	-38	0.042
131	JAK2	Janus protein-tyrosine kinase 2	-39	0.043
132	FIH (HIF1; HIF1AN)	Hypoxia-inducible factor 1-alpha inhibitor	-45	0.017
133	TRPC5 (TRP5)	Short transient receptor potential channel 5	-47	0.029
134	DUSP5	Dual specificity protein phosphatase-5	-49	0.040

135	WNK3 (PRKWNK3)	Protein-serine/threonine kinase WNK3	-51	0.045
136	Akt1 (PKBa)	RAC-alpha protein-serine/threonine kinase	-53	0.038
137	Grp75 (HspA9)	Stress-70 protein, mitochondrial	-59	0.008

List of the proteins with significant change in their expression levels following the treatment. %CFC attitudes change from control (%).